Phase Behavior and Self-Organized Structures in Water/Poly(oxyethylene) Cholesteryl Ether Systems

Takaaki Sato,[†] Md. Khalid Hossain,[‡] Durga P. Acharya,[‡] Otto Glatter,[§] Akio Chiba,[||] and Hironobu Kunieda*[,‡]

Division of Pure and Applied Physics, Graduate School of Science and Engineering, Waseda University, Okubo 3-4-1, Shinjuku-ku, Tokyo 169-8555, Japan, Graduate School of Environment and Information Sciences, Yokohama National University, Tokiwadai 79-7, Hodogaya-ku, Yokohama, 240-8501, Japan, Institute of Chemistry, University of Graz, Heinrichstrasse 28, A-8010 Graz, Austria, and Department of Applied Physics, School of Science and Engineering, Waseda University, Okubo 3-4-1, Shinjuku-ku, Tokyo 169-8555, Japan

Received: April 7, 2004; In Final Form: June 13, 2004

Different from conventional nonionic poly(oxyethylene) surfactants, poly(oxyethylene) cholesteryl ethers, $ChEO_n$, possess a bulky and nonflexible hydrophobic part and form a variety of self-organized structures in water. We investigated the phase behavior and the micellar structures in the water/$ChEO_{15}$ and water/$ChEO_{10}$ systems by means of visual observation, rheometry, small-angle X-ray scattering (SAXS), dynamic light scattering (DLS), dielectric relaxation spectroscopy (DRS), and densimetry. We found that in the water/$ChEO_{15}$ system, aqueous micellar (W_m), discontinuous micellar cubic (I_1) with *Fd*3*m* space group, hexagonal (H_1), rectangular ribbon (R_1), and lamellar (L_α) phases are formed, whereas W_m, unknown, R_1, defected lamellar (L_α^H), and L_α phases are produced in the water/$ChEO_{10}$ system at ambient temperatures. Compared with a conventional aqueous nonionic surfactant system, the intermediate R_1 phase region is incredibly wide. As for the water/$ChEO_{15}$ system, with increasing water content, the packing parameter, *P*, in the R_1 region is gradually decreased, finally converging to 1/2 at $W_s \sim 0.58$, indicative of the formation of the H_1 phase. The R_1 phase acts as a "distorted" hexagonal phase in the system. However, in the water/$ChEO_{10}$ system, upon reduction of W_S, *P* shows a steplike increase and the maximum value ∼0.67 at $W_S \sim 0.7$, just corresponding to the threshold of discontinuous and bicontinuous structures. After that, *P* is decreased with decreasing W_S and unknown phase that cannot be indexed to any known space group for liquid crystalline phases emerges at $W_S \sim 0.5$. The GIFT analysis of the SAXS data for the W_m solution indicates that spherical micelles are present in the water/$ChEO_{15}$ system in an ambient temperature range, but $ChEO_{10}$ forms a short-rod micelle in water. With increasing temperature, rodlike micelles appear to be grown and a viscoelastic micellar phase is formed in water/$ChEO_{10}$ system. The hydration number for each oxyethylene unit is evaluated as ∼4 by DRS, which gives a consistent explanation for the concentration dependence of the apparent hydrodynamic radius in the W_m phase obtained by DLS. Hydrated water molecules should be regarded as a constituent of the micelles. The majority of these features of novel phase behavior in the water/$ChEO_n$ systems are based on a nonflexible and bulky hydrophobic part of $ChEO_n$.

I. Introduction

Surfactant or amphiphilic molecules form an aggregate called micelle in water. When surfactants are sufficiently hydrophilic, they form spherical or short rod micelles. In some particular systems, especially, cetyl trimethylammonium bromide (CTAB) system, the micellar shape becomes enormously elongated and forms wormlike micelles, which shows viscoelastic behavior upon addition of KBr or salicylate salts.[1,2] Most of the studies on wormlike micelles are devoted to CTAB or cataionic surfactants related to the change in ionic repulsion of the headgroups in the presence of salt or other additives. However, recently, it was found that the highly viscoelastic wormlike micelles are also formed in nonionic surfactant systems, such as poly(oxyethylene) cholesteryl ether ($ChEO_n$) systems.[3] Cholesteryl frame is more bulky and rigid than conventional hydrocarbon chain. Hence, it is considered that one reason for the formation of wormlike micelles is attributed to its unique hydrophobic part. In the previous study, we used a combination of poly(oxyethylene) cholesteryl ethers and short-hydrophilic chain nonionic surfactant.[3]

In this context, we thoroughly investigated the temperature- and composition-dependent phase behavior of the water/poly(oxyethylene) cholesteryl ether ($ChEO_n$) binary systems (n = 10 and 15), employing several noble techniques. The phase diagrams as a function of temperature have been constructed. We were especially interested in how the phase behavior of the water/$ChEO_n$ systems is affected by the bulky hydrophobic cholesteryl group if compared with the phase behavior of the conventional water/C_mEO_n systems[4] and how the different hydrophobic/hydrophilic balance arising from the different length of hydrophilic oxyethylene chain in $ChEO_{10}$ and $ChEO_{15}$ influences the shape and size of micelles in the W_m phase and

* To whom correspondence should be addressed. Phone & Fax: +81-45-339 4190. E-mail: kunieda@ynu.ac.jp.
[†] Division of Pure and Applied Physics, Waseda University.
[‡] Yokohama National University.
[§] University of Graz.
[||] Department of Applied Physics, Waseda University.

10.1021/jp048469u CCC: $27.50
Published on Web 08/04/2004

SCHEME 1: Schematic Molecular Structure of $ChEO_n$

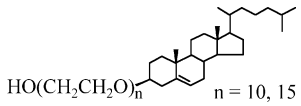

the total phase behavior. To explore these matters, we performed visual observation, small-angle X-ray scattering (SAXS),[5−15] rheometry,[3] dynamic light scattering (DLS),[16] dielectric relaxation spectroscopy (DRS),[17−20] and a precision densimetry.[21]

In this paper, we focus on the so-called "intermediate" liquid crystalline phases.[22−26] Various intermediate phases between hexagonal (H_1) and lamellar (L_α) phases have been identified in a number of surfactant-rich binary and ternary systems especially when the hydrophobic part of the surfactant molecule is large or rigid. In terms of topological symmetry, they can generally be classified into three types; rectangular ribbon (R_1), layered mesh (Mh_1), and possibly bicontinuous (V_1) structures.[22] All these structures can be characterized by their inhomogeneous interfacial curvature. Ionic systems more often show rich behavior in intermediate phases. Although it was reported that some D_2O/nonionic surfactant binary systems, such as $D_2O/C_{22}EO_6$[21] and $D_2O/C_{16}EO_6$,[24] exhibit layered mesh structures, the formation of rectangular ribbon phases in water/nonionic surfactant binary systems which we found in this study, is a quite unique phenomenon. The structural change in the aqueous micellar (W_m) phase is also of our great interest. The spherical-rodlike and the further rodlike-wormlike micellar transitions, and the relation between the shape of micelles in the W_m phase and a kind of crystal system of the liquid-crystalline phase next to the W_m region at higher surfactant concentrations will be extensively discussed.

II. Experimental Section

A. Materials. A-grade reagents of poly(oxyethylene) cholesteryl ether ($ChEO_n$; $n = 10$ and 15), where n is the number of repeated oxyethylene monomer units, were purchased from Nihon Emulsion Co., Japan, and used as received without further purification. Scheme 1 shows a constitutional formula of a $ChEO_n$ molecule.

B. Phase Diagrams. Samples of water/$ChEO_n$ binary systems ($n = 10$ and 15) at various concentrations were prepared by weighing the $ChEO_n$ reagents and Millipore water and sealed into ampules immediately after mixing. The concentration of the samples was defined by weight fraction of the surfactants, W_S. To attain homogeneity, the samples were thoroughly mixed using a vortex centrifuge by repeatedly passing through a narrow constriction of the ampules and kept in a thermostated water bath at 25 °C for several weeks. We made the phase identification of the water/$ChEO_{10}$ and the water/$ChEO_{15}$ systems for the entire concentration range in the temperature range $0 \le T/°C \le 100$ for the former and $0 \le T/°C \le 120$ for the latter by visual observation with crossed polarizers for checking optical anisotropy.

C. Small-Angle X-ray Scattering (SAXS). To examine the micellar shape and size in the W_m phase, SAXS measurements on 1, 5, 10, 15, and 20 wt % water/$ChEO_n$ ($n = 10$ and 15) binary systems were carried out at 25 °C in Institute of Chemistry, University of Graz, Austria, using a SAXSess camera (Anton Paar, Austria), equipped with a focusing multilayer optics, a block collimator for a slit collimation, a transparent beam stop, and an IP detector (Fuji BAS 1800 from Raytest, Straubenhardt, Germany). All of the SAXS data for the W_m solutions were obtained in an absolute scale with a standard deviation at each q, required for the weighted least-squaresd quantitative analysis. Water was successfully used as a secondary standard for the absolute intensity calibration.[15] Owing to a transparent beam stop of the SAXSess apparatus, the raw scattering data always include a reduced primary intensity at $q = 0$. The $q = 0$ intensity, $I(0)$, was routinely normalized into unity for the calibration of transmission. This advanced procedure makes the absolute intensity calibration easy, quick, and accurate.

The spatially averaged q-dependent scattering intensity, $I(q)$, can be given by the Fourier transform of the pair distance distribution function (PDDF) of the particle, $p(r)$

$$I(q) = 4\pi \int_0^\infty p(r) \frac{\sin qr}{qr} \, dr \tag{1}$$

The intraparticle scattering contribution is connected to the form factor, $P(q)$, and the interparticle one to the structure factor, $S(q)$. For monodisperse spherical systems, the total scattering, $I(q)$, can simply be given by

$$I(q) = nP(q)\, S(q) \tag{2}$$

with n being the particle density. For polydisperse spherical and even polydisperse nonspherical systems, a similar expression to eq 2 can be validly applied by replacing $S(q)$ by the effective structure factor, $S^{eff}(q)$ considering not only the particle distribution in space but also the form amplitudes of the particles.

The obtained SAXS data were processed by the generalized indirect Fourier transformation (GIFT) method.[7,12−14] In the semidilute region, where volume fraction is greater than ~1%, apparently particle interactions are not negligible. The GIFT method allows us to determine the form factor and the structure factor simultaneously from the scattering data obtained in the absolute scale without any assumption on the structure of the particles (form factor). The available minimum q value for the GIFT calculation was carefully checked by the Guinier plot, and the desmeared data typically in the range of $\sim 0.07 \le q/nm^{-1} \le 5.0$ were used for the series of the analysis.

For the liquid crystalline phases, further crystal-system characterization was performed with the help of SAXS by the use of a NANO−Viewer (Rigaku-denki, Japan), composed of a 0.8 kW anode rotating X-ray generator (MicroMax007), a point-convergence confocal mirror (Confocal Max-Flux) for a pinhole collimation, and a CCD detector. The samples inserted into a slot of a metal sample holder were covered with thin Mylar films. The SAXS data were obtained at about 25 °C in an arbitrary unit, and the peaks were crystallographically analyzed for determination of the types of crystal system of the liquid-crystalline phases and a quantitative estimation of the interlayer spacing.

The volume fraction of lipophilic part of surfactant was calculated using the following equation:

$$\phi_L = \frac{V_L}{V_S + \dfrac{M_S}{\rho_W} \dfrac{1 - W_S}{W_S}} \tag{3}$$

where V_S and V_L are the molar volumes of surfactant and its lipophilic part, ρ_W is density of water, M_S is the molecular weight of surfactant, and W_S is the weight fraction of surfactant in the binary system. To obtain more detailed geometrical information of liquid crystalline structures from the interlayer spacing, d, we assumed the following equations to evaluate the

length of hydrophobic part, d_L, for the L_α, H_1, and I_1 phases respectively

$$d_L = \frac{\phi_L}{2} d \tag{4}$$

$$d_L = \left[\frac{2}{\sqrt{3}\pi}\phi_L\right]^{1/2} d \tag{5}$$

and

$$d_L = \left[\frac{3\phi_L}{4\pi n_C}\right]^{1/3} \sqrt{h^2 + k^2 + l^2}\, d_{hkl} \tag{6}$$

where h, k, and l are the Miller indices, n_C is the number of the particle in a unit cell, and $h^2 + k^2 + l^2 = 3$ for a face-centered, 2 for a body-centered, and 1 for a simple cubic array.

The packing parameter[27−29] defined as $P = v_L/a_S d_L$, where v_L is the volume of hydrophobic part and a_S is the effective cross sectional area per surfactant molecule, is 1, 1/2, and 1/3 respectively for the L_α, H_1, and I_1 phases. Then a_S in the L_α, H_1, and I_1 phases can be respectively related to d as

$$a_S = \frac{2v_L}{d}\frac{1}{\phi_L} \tag{7}$$

$$a_S = (2\sqrt{3})^{1/2}\frac{v_L}{d}\left(\frac{1}{\phi_L}\right)^{1/2} \tag{8}$$

and

$$a_S = (36\pi)^{1/3}\frac{n_C^{1/3}}{\sqrt{h^2 + k^2 + l^2}}\frac{v_L}{d}\left(\frac{1}{\phi_L}\right)^{1/3} \tag{9}$$

where n_C is the number of micelles in a unit cell.

For a two-dimensional rectangular lattice,[30] the Bragg reflections are given by the magnitude of the scattering vector

$$q_{hk} = 2\pi\left(\frac{h^2}{a^2} + \frac{k^2}{b^2}\right)^{1/2} \tag{10}$$

where h and k are the Miller indices for the planes, and a and b are the dimensions of the unit cell ($b > a$). For the primitive rectangular symmetry, *pgg*, together with the restrictions, $h = 2n$ for (h0) and $k = 2n$ for (0k), any positive integer is available for h and k, and for the centered rectangular symmetry, *cmm* or *cm*, the Miller indices, h and k, should satisfy the condition of $h + k = 2n$. The lattice parameters, a and b, can be determined from the two smallest scattering vectors, q_{02} and q_{11}.

For the intermediate Ribbon (R_1) phase, we used a hexagon-rod model[31,32] with the length of the lamellar-like part, $2L$, for which a constant layer thickness for hydrated hydrophilic part is assumed. The length of the smallest dimension of the aggregate, d_L, can be evaluated form

$$d_L = \frac{1}{4\sqrt{3}}[\{(b - \sqrt{3}a)^2 + 4\sqrt{3}ab\phi_L\}^{1/2} - (b - \sqrt{3}a)] \tag{11}$$

and the axial ratio of the aggregate, ρ_A, is given by

$$\rho_A = \frac{d_L + L}{d_L} = 1 + \frac{b - a\sqrt{3}}{4d_L} \tag{12}$$

To calculate the effective cross sectional area per surfactant molecule, a_S, a hemicircular capped rectangle for the ribbonlike aggregate with the same d_L value as for the hexagon-rod approximation is considered. Then a_S is obtained as

$$a_S = v_L\left[\frac{1}{d_L} + \frac{2\pi}{b + (4d_L - a)\sqrt{3}a}\right] \tag{13}$$

D. Dynamic Light Scattering (DLS). The dynamic light scattering measurements on 1, 5, 10, 15, and 20 wt % aqueous solutions of $ChEO_n$ ($n = 10$ and 15) at 25 °C were performed by the use of a laboratory built goniometer equipped with an Ar^+ laser (514.5 nm, BeamLok 2060−5S, Spectra Physics, Darmstadt, Germany)[16] at Institute of Chemistry, University of Graz. The detection optics consisted of a single mode fiber (OZ from GMP, Zürich, Switzerland) coupled to an ALV/SO-SIPD/DUAL photomultiplier with pseudo cross-correlation setup, ALV-5000 multiple tau digital correlator with ALV-5000/FAST extension (all from ALV, Langen, Germany). The sample cell, a 10 mm cylindrical cuvette, was immersed in a thermostated index matching bath filled with Decaline solvent. Basically, the laser intensity of ∼150 mW was chosen, and the temperature was controlled within an accuracy of ±0.1 °C. A fluctuating scattered signal, $I(t)$, is connected to the diffusion of particles. The intensity autocorrelation function (ACF)

$$G_2(\tau) = \langle I(0)I(\tau)\rangle = \lim_{T\to\infty}\frac{1}{T}\int_0^T I(t)I(t+\tau)\,\mathrm{d}t \tag{14}$$

The effective diffusion coefficient, D_{eff}, was deduced by the $q \to 0$ extrapolation of $\Gamma(q)/q^2$, where q is the scattering vector and Γ the decay rate of the normalized electric field correlation function, $G_1(t)$. The hydrodynamic radius of micelles in the solutions, R_H^{app}, was calculated from D_{eff}, referring to the Stokes−Einstein equation

$$R_H^{app} = \frac{k_B T}{6\pi\eta_S D_{eff}} \tag{15}$$

where k_B is the Boltzmann constant, T is the absolute temperature, and η_s is the solvent (water) viscosity.

E. Rheological Measurements. Steady shear-rate and oscillatory-shear (dynamic) rheological measurements were performed for a 2.5 wt % $ChEO_{10}$ aqueous solution in the temperature range $25 \le T/°C \le 65$ using an ARES rheometer (Rheometric Scientific) with a couette geometry (cup diameter: 34 mm, bob diameter: 32 mm, bob length: 33.3 mm). At higher temperatures, the solution was equilibrated at least for 30 min before starting the measurement. A lid was used to cover the sample so as to minimize a change of the sample composition by evaporation. Dynamic frequency sweep measurements were performed in linear viscoelastic regime of the samples, as determined previously by dynamic strain sweep measurements. The zero-shear viscosity is estimated by extrapolating the viscosity curves of steady or dynamic measurements to zero shear-rate or zero shear-frequency.

F. Dielectric Relaxation Spectroscopy (DRS). Dielectric relaxation spectroscopy (DRS)[17−20] can monitor the cooperative motion of a molecular ensemble through the response of the total dipolar moment of the samples to a time-dependent electric field. To get information about hydration of the oxyethylene (EO) chain and states of water in the binary systems from the viewpoint of molecular dynamics, we determined the complex dielectric spectra of 5, 10, and 15 wt % water/$ChEO_n$ binary systems ($n = 10$ and 15) at 25 °C in the frequency range $0.1 \le \nu/GHz \le 20$ by the use of time domain reflectometry (TDR).[17−19]

The advanced technique, the time-window divided modified direct (TDMD) method[19] with two different cell constants was employed to increase the resolution of the measurements and simultaneously to achieve a sufficient low-frequency limit.

With a nonlinear least-squares fitting procedure we thoroughly tested various conceivable relaxation models based on a superposition of n Havriliak−Negami (HN) equations, or its variants

$$\epsilon^*(\nu) = \epsilon_\infty + \sum_{j=1}^{n} \frac{\Delta\epsilon_j}{[1 + (i2\pi\nu\tau_j)^{\beta j}]^{\alpha j}} \qquad (16)$$

to fit the experimental $\epsilon^*(\nu)$ spectra after subtraction of a small contribution from DC conductivity of the samples. In the models, the jth dispersion step ($j = 1, 2, ..., n$) is defined by its relaxation time, τ_j ($\tau_j > \tau_{j+1}$) and relaxation amplitude, $\Delta\epsilon_j$, where n is the number of the separable dispersion steps. ϵ_∞ is the infinite frequency permittivity, and α_j and β_j are the shape parameters representing an asymmetric and a symmetric shape of a spectrum, respectively.

G. Densimetry and Sound Velocity Measurements. Using a high precision densimeter, DMA5000 (Anton Paar, Austria),[21] a precision densimetry and sound velocity measurements were carried out on 5, 10, 15, and 20 wt % water/ChEO$_n$ (n = 10 and 15) binary solutions in the temperature range $5 \le T/°C \le 70$. The highly tuned temperature control of the apparatus makes an accuracy of 10 mK in an absolute value possible. The temperature was scanned with an increment of 1.0 K by an automatic temperature scan mode. For densimetory, a DMA 5000 instrument is based on the conventional mechanical oscillator method, which measures the natural resonant frequency of a U-shaped glass tube filled with 1 mL sample, and sound velocity can be obtained by a pulse technique measuring the time which a short pulse with a center frequency of 3 MHz takes to pass through a 5 mm distance in the sample. It is expected that the analysis of the temperature dependence of these quantities give us information about temperature-induced structural changes in the W_m phase.

III. Results and Discussion

A. Phase Behavior of the Water/ChEO$_n$ Binary Systems. The phase diagram of the water/ChEO$_{15}$ and the water/ChEO$_{10}$ binary systems as a function of temperature is displayed in Figure 1, and typical SAXS spectra for liquid crystalline phases are displayed in Figure 2. Due to the intricate balance between the effects of hydrophobic part and hydrophilic part induced by the different oxyethylene (EO) chain lengths and their relative change depending on temperature and water content, the water/ChEO$_{10}$ and the water/ChEO$_{15}$ systems show fairly different phase behavior, the water/ChEO$_{15}$ showing rather straightforward one compared with that of the water/ChEO$_{10}$.

The present phase diagrams show that, in common for the water/ChEO$_{10}$ and the water/ChEO$_{15}$ systems, the surfactant layer curvature gradually becomes more positive with increasing water content. Here we define the positive curvature as the convex surfactant layer toward water layer in aggregates, corresponding to normal-type self-organized structures. In Figure 3, we display (a) the interlayer spacing, d, for liquid crystalline phases and (b) the effective cross sectional area per surfactant molecule, a_S, and the length of hydrophobic part, d_L, in the water/ChEO$_n$ (n = 10 and 15) systems as a function of W_S, at 25 °C. Surprisingly, the water/ChEO$_{15}$ and the water/ChEO$_{10}$ systems show very similar d values despite a large difference

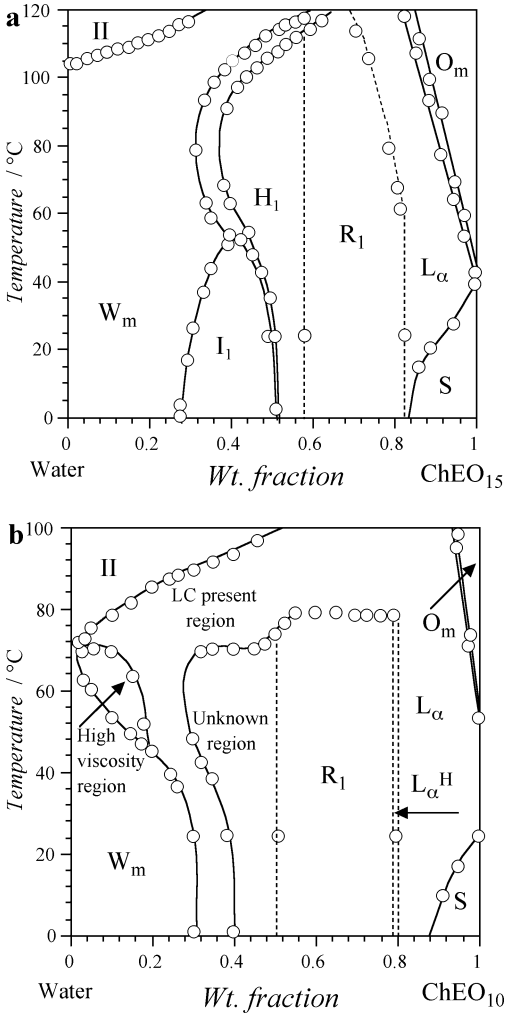

Figure 1. Phase diagram of the binary water/ChEO$_n$ (n = 10 and 15) systems as a function of temperature and surfactant weight fraction, W_S. W_m, I_1, H_1, R_1, L_α^H, L_α, and O_m denote aqueous micellar, micellar cubic, hexagonal, intermediate ribbon, distorted lamellar, lamellar, and reverse micellar phases, respectively. S is a solid-present region, and II indicates a two-phase region.

of the EO chain length. Compression of the EO chain and a packing scheme of surfactant molecules are balanced and compensated with each other. The smaller a_S for the water/ChEO$_{10}$ system shows that ChEO$_{10}$ molecule with shorter EO chain, and, in consequence, more pronounced hydrophobicity, prefers tighter packing than ChEO$_{15}$ molecule. In the L_α phase, ChEO$_{15}$ shows the smaller d_L than that of ChEO$_{10}$. The arrangement of hydrophobic part of ChEO$_{15}$ molecules seems to be slightly tilted against the perpendicular axis to the lamellar layers.

Both water/ChEO$_{15}$ and the water/ChEO$_{10}$ systems exhibit an extensive intermediate phase region. In general, the intermediate phases are often found between the H_1 and L_α phases.[22−26] However, the H_1 phase is missing in the water/ChEO$_{10}$ system. When W_S is reduced from the R_1 phase region, instead of the H_1 phase, an unknown phase that cannot be assigned to any space group of known liquid crystalline phases is produced at $W_S \sim 0.52$. Although in terms of the peak position, W_s=0.5 might be categorized into R_1 phase, the stronger higher order reflection is not well explained. The I_1 phase is also formed only in the water/ChEO$_{15}$ system. The three reflections in the positional ratio of $\sqrt{3}:\sqrt{8}:\sqrt{12}$ could be indexed to the (111), (220), and (222) planes of *Fd*3*m* space group, the typical space group for the discontinuous micellar

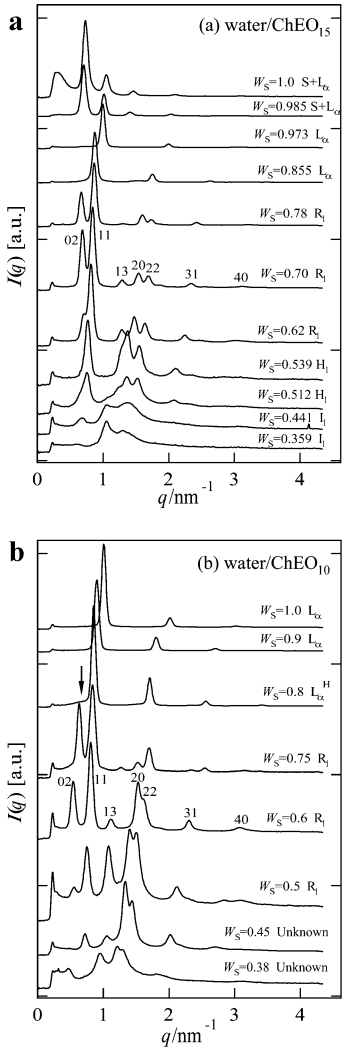

Figure 2. Typical SAXS spectra for the liquid crystalline phases in (a) the water/$ChEO_{15}$ system and (b) the water/$ChEO_{10}$ system. The phase notations are the same as Figure 1.

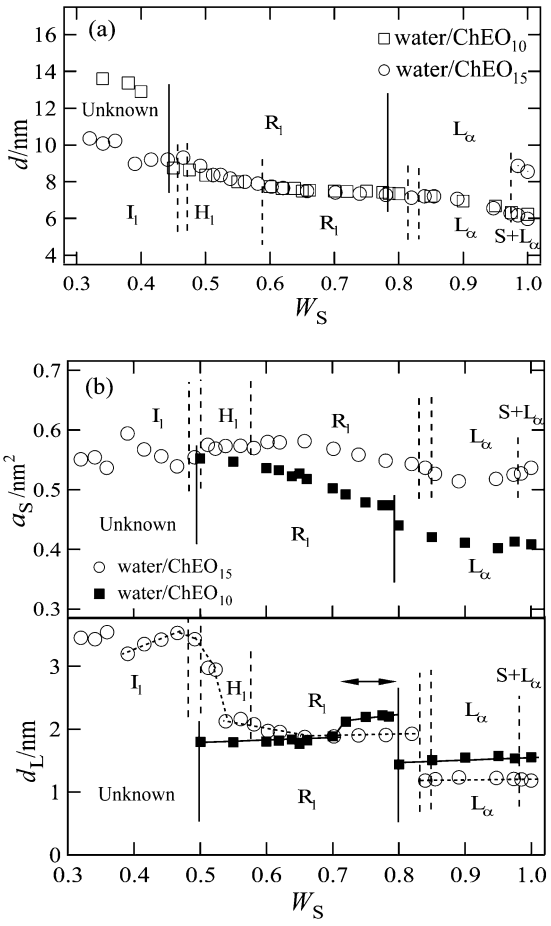

Figure 3. Concentration dependence of (a) the interlayer spacing, d, for liquid crystalline phases, and (b) the effective cross sectional area per surfactant molecule, a_S, and the length of hydrophobic part of a surfactant molecule in the water/$ChEO_n$ ($n = 10$ and 15) systems as a function of the weight fraction of surfactant W_S at 25 °C.

cubic (I_1) phase.[5,6] The I_1 phase directly touches the aqueous micellar (W_m) phase in which spherical micelles are present according to the SAXS results with the GIFT calculation, as we will discuss in section III.C. This supports the identification of the I_1 phase composed of discrete spherical micelles. The maximum temperature of the I_1 phase in the water/$ChEO_{15}$ system is around 52 °C. With increasing surfactant concentration, the hexagonal (H_1) phase is produced via a narrow two phase region around 52 wt % of $ChEO_{15}$. Four reflections in the positional ratio of $1:\sqrt{3}:\sqrt{4}:\sqrt{7}$ observed here are just the expected signature for the H_1 phase. Although a three-phase region among the I_1, H_1 and W_m domains can be expected, it is difficult to identify by visual observation. With the further increase of W_S, the H_1 phase is successively changed into the intermediate R_1 phase at ca. 58 wt % of $ChEO_{15}$. The H_1-R_1 phase transformation is attributed to an increasing packing constrain caused by the bulky sterol moiety in the lipophilic core due to which the circular cross-section of the lipophilic core of the H_1 phase gets elongated. The evolution of the SAXS pattern from the H_1 to R_1 phase (Figure 2a) suggests a gradual elongation of the cross-section of the lipophilic core of the rodlike aggregate with increasing W_S. The two-phase region between the H_1 and R_1 phase could not be located probably because macroscopic phase separation does not occur due to close similarity in the structure. On the basis of the SAXS pattern at 25 °C, the tentative phase boundary between the H_1 and R_1 phase in the phase diagram (Figure 1a) is shown by a dotted line. The detail of the structure of the R_1 phase will be discussed in the next section. Finally the lamellar (L_α) phase is produced at ca. 83 wt %. A reverse micellar solution phase (O_m) is also formed above the solid present (S) phase at higher temperature. The melting temperature of the poly(oxyethylene) cholesteryl ether is largely decreased with increasing water content due to the hydration of EO chain.

As can be seen in Figure 2a, neat $ChEO_{15}$ and a 98.5 wt % $ChEO_{15}$ in water exhibit up to four reflections. The first and third peaks and the second and fourth peaks from the low-q side are respectively in the positional ratio of 1:2, indicating a two-lamellar coexisting state. These pairs respectively give the interlayer spacings, $d^S = 8.5$ nm and $d^{L\alpha} = 6.2$ nm. When the EO chain length is increased, the melting temperature of solid is predominantly determined by the melting temperature of the poly(oxyethylene) chain. Although a small amount of impurity water may affect the melting point of the neat $ChEO_{15}$, the system partly remains in the solid state due to its relatively high melting point, and the ordered trans conformation of the EO chain in the solid produces the wider interlayer spacing. However, as shown in Figure 2, when a small amount of water is added, the first and third reflections related to $d^S = 8.5$ nm suddenly disappear, and subsequently, the intensity of the second and fourth peaks with $d^{L\alpha} = 6.2$ nm attributed to the liquid crystalline lamellar (L_α) phase become rapidly strong. The melting temperature of the poly(oxyethylene) cholesteryl ether

is largely decreased with increasing water content due to the hydration of EO chain. At $W_S < 0.98$, the reflections from solid can no longer be observed.

In the water/$ChEO_{10}$ system, with increasing W_S, the W_m phase, in which short rodlike micelles appear to be produced, is transformed into a transparent, birefringent, and viscous liquid crystalline phase at $W_S \sim 0.38$ via a turbid and less viscous two-phase region which extends over ~10 wt %. The SAXS pattern of this liquid crystalline phase, as is shown in Figure 2b ($W_S = 0.38$ and 0.45), cannot be fitted to any space group of well-known liquid crystalline phases. To ensure that SAXS pattern of the unidentified region is not due to insufficient mixing, the samples were left for equilibration for several weeks after they were thoroughly mixed by repeated centrifugation for several days. The SAXS patterns of the "unknown liquid crystalline phase" suggest a structural evolution with increasing concentration of surfactant, leading to the formation of R_1 phase at $W_S \sim 0.5$. The liquid crystalline phase located between the W_m phase of rodlike micelles and the R_1 phase is expected to be composed of long rodlike aggregates, although the detailed structure of the phase is not known. It is possible that due to the bulky lipophilic (sterol) group, the cross-section of the rodlike aggregate in this unknown phase is not circular as in the aggregates of the H_1 phase, but they are already distorted to an elliptical shape and show an unknown spatial arrangement.

After showing fairly different behavior of the axial ratio of the ribbonlike aggregates from that in the water/$ChEO_{15}$ system, the R_1 phase is changed into the L_α phase at $W_S \sim 0.8$. In a narrow region close to the R_1-L_α boundary, as indicated by an arrow in Figure 2b, a bump on the low-q side of the first-order reflection from the lamellar structure appears, which is a signature of a defected lamellar (L_α^H) phase.[26] At high temperatures, "unknown liquid crystal" and the R_1 phases transform to a birefringent and turbid but less viscous solution, as indicated by 'LC present region' in the phase diagram (Figure 1b). The boundary of this "LC present region" in the water-rich as well as surfactant-rich regions were not able to be ascertained by visual observation. A narrow O_m region is also observed at higher temperature above the solid present (S) phase region.

B. Intermediate Ribbon (R_1) Phase. A particular feature of the intermediate phase is the sudden appearance of a strong low-q reflection, when the surfactant concentration is decreased from the lamellar (L_α) phase region.[22−26] As Figure 2 shows, the strong first-order reflection from the L_α phase is continuous with the second reflection in the intermediate phase which is indexed to the (11) plane of the two-dimensional rectangular lattice. This indicates that the second reflection comes from an interlayer spacing. We also tested other possible intermediate structures, e.g., by indexing the first and second strong reflections respectively to (101) and (002) planes of a tetragonal mesh structure, and (110) and (003) planes of a rhombohedral mesh structure, but higher order reflections cannot be fitted to these structures. Only a two-dimensional rectangular lattice can give a convincing explanation to the SAXS pattern characterized by the two strong low-q reflections supplemented by up to six other small reflections. Scheme 2 shows a schematic structure of the R_1 phase with a *cmm* symmetry.

Using eq 10, the lattice parameters, a and b, for the ribbonlike aggregates can be evaluated from the q-vectors of the two low-q reflections, q_{02} and q_{11}, as

$$q_{02} = \frac{4\pi}{b} \tag{17}$$

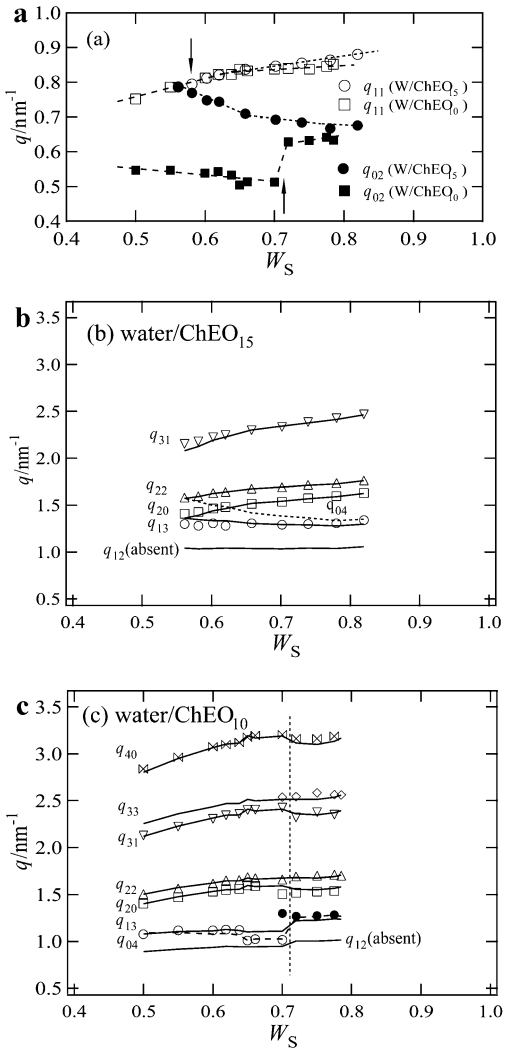

Figure 4. Concentration dependence of the q-vectors obtained form the SAXS measurements for the R_1 phase; (a) q_{02} and q_{11} for the water/$ChEO_{10}$ and water/$ChEO_{15}$ systems, (b) q_{hk} of the higher order reflections for the water/$ChEO_{15}$ system, and (c) those for the water/$ChEO_{10}$ system.

SCHEME 2: Schematic Structure of the R_1 Phase with a *cmm* Symmetry with the Unit Cell Parameters *a* and *b*

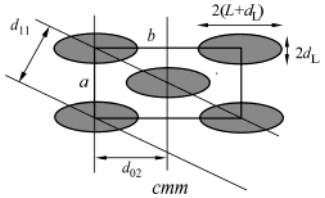

and

$$q_{11} = 2\pi\left(\frac{1}{a^2} + \frac{1}{b^2}\right)^{1/2} \tag{18}$$

and then the q vectors for other planes can be calculated assigning the values of a and b into eq 10. Figure 4 shows the concentration dependence of the q vectors in the R_1 phase; (a) q_{02} and q_{11} for the water/$ChEO_{10}$ and water/$ChEO_{15}$ systems, (b) q_{hk} of the higher order reflections for the water/$ChEO_{15}$ system, and (c) that for the water/$ChEO_{10}$ system. The absence of the reflection from the (12) plane clearly shows that the primitive recutagular space group, *pgg*, is not the case for the investigated systems. The intermediate phase can be identified

as the recutangular ribbon (R_1) phase with the centered rectangular symmetry, *cmm* or *cm*. We think that it is better not to be decisive for the symmetry because the SAXS data do not give any direct information about which symmetry, *cmm* or *cm*, is appropriate. Taking a general packing requirement with a constant hydrophilic layer thickness into account, a *cmm* symmetry could be preferably assumed. However, considering the fact that the first-order reflection from the L_α phase is smoothly taken over by the reflection from the (11) plane of the R_1 phase, just after the formation of the R_1 phase form the L_α phase, the arrangement of the ribbonlike aggregates may be tilted against the long axis of the rectangular if it remains parallel with the lamellar layers as a vestige of the L_α phase. In this case the structure cannot be categorized into a *cmm*, but can into a *cm* symmetry.

Being quite interesting and important, the concentration dependence of the peak position of the two low-q reflections for the water/$ChEO_{10}$ and water/$ChEO_{15}$ systems exhibits completely different trends, as shown in Figure 4a. In the case of the water/$ChEO_{15}$ system, with decrerasing W_S, q_{11} (corresponding to the interlayerspacing) and q_{02} (reflecting the long axis of the rectangular lattice) respectively shift to the lower and higher values, and the peak from the (02) plane finally merges into that from the (11) plane at $W_S \sim 0.58$. At the same time, the peak from the (13) plane also merges with that form the (22) plane. The (11) and (02) planes and the (13) and (20) planes for the recutangular structure respectively become the (10) and (11) planes for the hexagonal (H_1) structure at $W_S \sim 0.58$.

The packing parameter approach[27−29] is simple but in many case quite useful. The packing parameter, P, for the L_α and H_1 are 1 and 1/2, respectively. $1 > P > 2/3$ is the region of bicontinuous cubic (V_1) phase, and from $P = 2/3$ to 1/2, discontinuous intermediate phase, such as mesh (Mh_1) phase and ribbon (R_1) phases, are formed. Note that both V_1 phase and discontinuous intermediate phases are not often observed in water/surfactant systems even when encompassing very wide range of the packing parameters. Using a hexagon-rod model, we evaluated the axial ratio of the ribbonlike aggregate, ρ_A, and the packing parameter, P. In Figure 5, ρ_A and P are plotted against W_S, together with the dimensions of the rectangular unit cell, a and b, and their ratio, b/a. With decreasing W_S in the R_1 region, ρ_A for the water/$ChEO_{15}$ systems successively decreases, corresponding to a gradual increase of the mean interfacial curvature, going from $\rho_A \sim 1.7$ at $W_S \sim 0.82$ (close to the L_α to R_1 boundary) to $\rho_A \sim 1$ at $W_S \sim 0.58$ (the R_1 to H_1 boundary), indicative of an almost circular cross section of the cylindrical aggregates. The calculated packing parameters for the R_1 phase are in the range of $1/2 < P < 2/3$, as expected for discontinuous intermediate structures. P monotonically decreases with decreasing W_S, and becomes very close to ~0.5, again the signature of the H_1 phase, at $W_S \sim 0.58$. We can thus conclude that the R_1 phase in the water/$ChEO_{15}$ system, which covers a substantial region, ranging from ca. 58% to ca. 83 wt %, acts as a "distorted" hexagonal phase. With increasing water content, the interfacial curvature increases and it becomes less inhomogeneous, and the "distortion" gradually disappears, which seems to imply thermodynamically the second-order phase transition for the R_1 to the H_1 transition, being different from the L_α to R_1 and the H_1 to I_1 transitions.

In the water/$ChEO_{10}$ system, due to a different HLB, a pronounced hydrophobicity of the $ChEO_{10}$ molecule with the shorter EO chain, the behavior of all the parameters characterizing the unit cell and aggregates is not straightforward

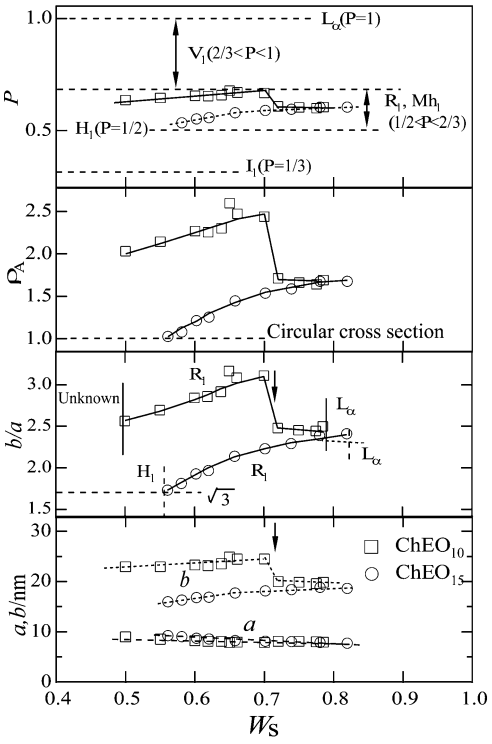

Figure 5. Concentration dependence of the structural parameters characterizing the ribbon (R_1) phase; the dimensions of the rectangular unit cell, a and b, the ratio, b/a, the axial ratio of the ribbonlike aggregate, ρ_A, and the packing parameter, P, plotted against the surfactant weight fraction, W_S, where ρ_A and P were calculated applying the hexagon-rod model.

compared with that in the water/$ChEO_{15}$ system. The axial ratio of the aggregates, ρ_A, shown in Figure 5, is nearly constant in $0.78 \geq W_S \geq 0.72$ despite the decrease of W_S, which is in parallel with the almost constant lattice parameters a and b. In this region, as shown in Figure 3, d_L exhibits larger values than that in the remaining R_1 region. A striking finding is that at $W_S \sim 0.72$, ρ_A and P show a steplike increase, indicating a sudden growth of the aggregates in the direction of the long axis of the ribbon structure, which is revealed by a sudden positional shift of the reflection from the (02) plane to the lower-q value at this concentration. At $W_S \sim 0.7$, P reaches the maximum value of ~0.67, just corresponding to the threshold between bicontinuous and discontinuous intermediate regions as shown in Figure 5.

In contrast to the situation in the water/$ChEO_{15}$ system, the peaks from the (11) and (02) planes do not merge into one peak but are separately observed for the entire R_1 region, whereas the reflection from the (02) plane gradually fade when W_S approaches ~0.5, and a background of the SAXS spectrum becomes larger, indicative of the formation of highly distorted inhomogeneous structures. In the region of $0.72 \geq W_S \geq 0.5$, ρ_A is again decreased with decreasing W_S, and finally unknown phase whose SAXS peaks cannot be indexed to any known space group for liquid crystal is formed at $Ws \sim 0.5$. In general, the surfactant layer curvature increases from negative to positive with decreasing surfactant content, so the steplike increase of ρ_A and P, corresponding to a sudden decrease of the surfactant layer curvature despite decreasing surfactant content, is quite unique phenomenon in a water/surfactant binary system. In $0.78 \geq W_S \geq 0.72$, less elongated and "loosely" packed ribbon aggregates with a large d_L are formed, and at $W_S \sim 0.72$, a sudden compression in the direction of the short axis and elongation in that of the long axis of aggregates occur. However,

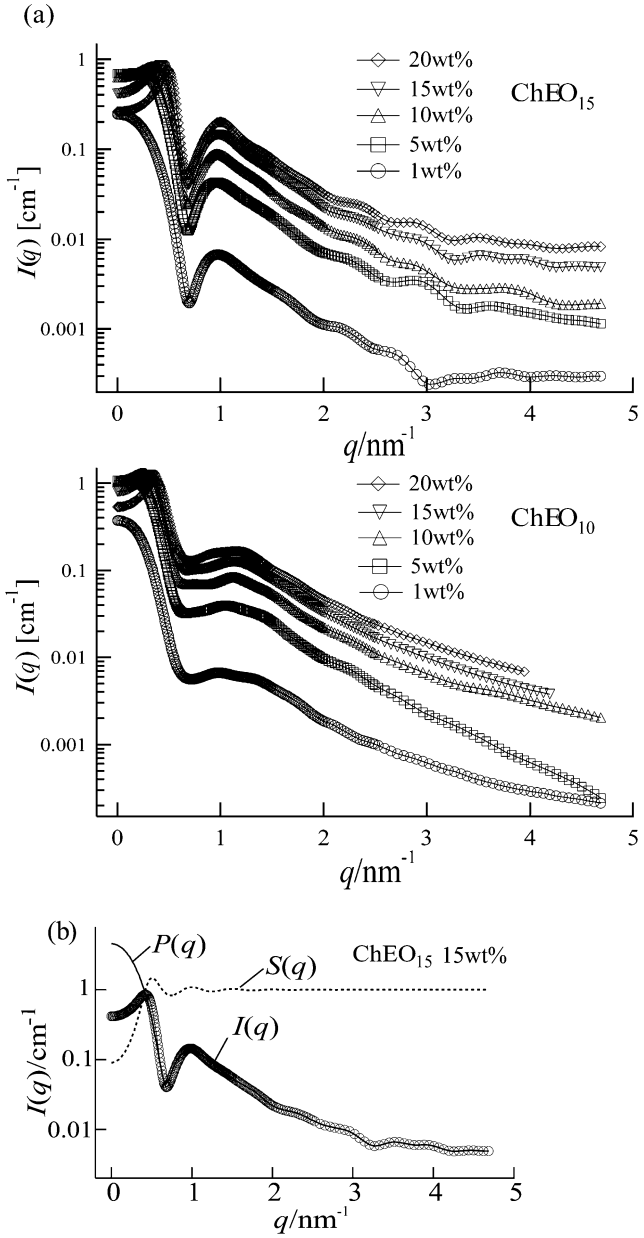

Figure 6. (a) SAXS curves of the 1, 5, 10, 15, and 20% water/$ChEO_{10}$ and water/$ChEO_{15}$ solutions as a function of the q vector obtained in an absolute unit at 25 °C. (b) demonstrates the separation of the form factor, $P(q)$, and the (effective) structure factor, $S(q)$, from the scattering intensity, $I(q)$, by the use of the GIFT method.

the packing parameter, P, cannot exceed 2/3 and it decreases with decreasing W_S, as is expected. The question still remaining to be answered here is, what is the driving force that wins a competition with the hydrophilic headgroup repulsion induced by an increase of water fraction.

C. Aqueous Micellar (W_m) Phase. We investigated the W_m phase in the water/$ChEO_{15}$ and the water/$ChEO_{10}$ binary systems by the combinational use of SAXS, rheology, DLS, DRS, and densimetry to examine the micellar shape and size.

A series of scattering curves of the water/$ChEO_{15}$ and the water/$ChEO_{10}$ solutions obtained in an absolute unit are shown as a function of the weight fraction of the surfactant, W_S in Figure 6a. In appearance, the water/$ChEO_{15}$ system exhibits a signature of the scattering curve from a spherical particle, whereas the water/$ChEO_{10}$ systems show more smeared one. Interparticle interactions can nearly be neglected at the lowest concentration of W_S=0.01. However, with increasing surfactant

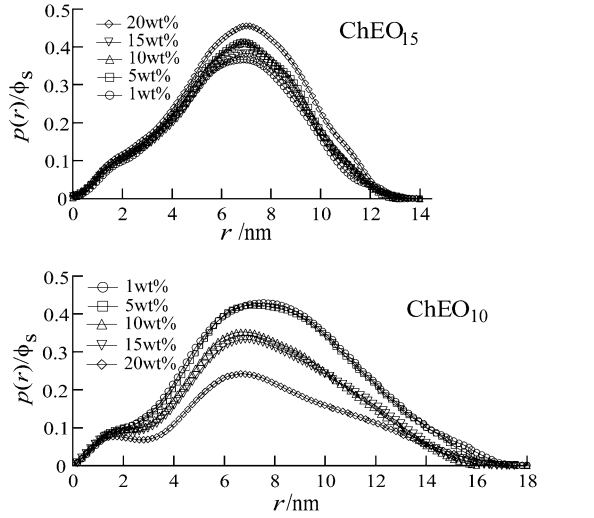

Figure 7. Pair distance distribution functions (PDDFs) of the 1, 5, 10, 15, and 20% water/$ChEO_{10}$ and water/$ChEO_{15}$ solutions normalized by the volume fraction of the surfactant at 25 °C.

concentration, the normalized SAXS intensity by the surfactant concentration, $I(q)/\phi_S$, shows a marked decrease in the forward scattering and the growth of the so-called interaction peak can clearly be observed.

These SAXS data were processed by the GIFT method, which, as shown in Figure 6b, allows us to separate the form factor $P(q)$ and the structure factor $S(q)$. In Figure 7, we display the pair distance distribution function (PDDF) for $ChEO_{15}$ and $ChEO_{10}$ normalized by the actual concentration of the surfactants, $p(r)/\phi_S$. The PDDF corresponds to the form factor $P(q)$ in real space. The normalized PDDFs for $ChEO_{15}$ are nearly unchanged irrespective of a large variation of W_S, giving the maximum dimension of the particle, $D_{max} \sim 13$ nm. This indicates that a shape and size of micelles are virtually kept unchanged in the wide composition range of $0 < W_S \leq 0.2$. A symmetric bell-like shape of the PDDFs for $ChEO_{15}$ strongly suggests the presence of nearly spherical particles with an approximate radius of 6.5 nm. In contrast, the normalized PDDFs for $ChEO_{10}$ show the features of a nonspherical particle, such as two maxima in $p(r)/\phi_S$ and asymmetric shape with an extended tail in high-r region. Note that the first small peak (bump), which is a signature of the internal inhomogeneity, is also visible in $ChEO_{15}$, but less pronounced. The finding that $D_{max} \sim 16-17$ nm for $ChEO_{10}$ with a shorter oxyethylene chain which exceeds that of $ChEO_{15}$ by ~20%, together with the ratio of D_{max} to r_{max} (a position of the maximum) of $ChEO_{10}$ largely exceeding two, is highly indicative of the formation of elongated micelles, possibly short-rod micelles. To determine the geometry of the particle in the water/$ChEO_{10}$ systems in more specific way, we will need the SANS measurements for the better contrast.

In Figure 8, the structure factors, $S(q)$, for the water/$ChEO_{15}$ and water/$ChEO_{10}$ systems are displayed. $S(q)$ is given by Fourier transform of the total correlation function as

$$S(q) - 1 = 4\pi n \int_0^\infty [g(r) - 1] r^2 \frac{\sin qr}{qr} \, dr \qquad (19)$$

We used a hardsphere (HS) interaction potential for nonionic micellar systems. In the HS model, the interaction radius, the volume fraction, and the polydispersity are the output of the fitting procedure (Boltzmann-simplex-simulated annealing).[14]

The $S(0)$ value rapidly decreases with increasing W_S, indicating the lower isothermal compressibility of the systems cor-

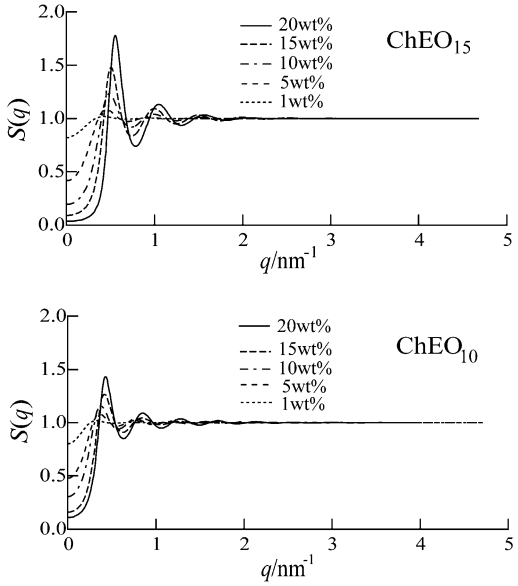

Figure 8. (Effective) structure factor, $S(q)$, of the 1, 5, 10, 15, and 20% water/$ChEO_{10}$ and water/$ChEO_{15}$ solutions at 25 °C as a function of the q vector.

related with pronounced repulsive interactions between the particles for the higher concentration. As for the water/$ChEO_{15}$ system, the interaction peak becomes sharper and shifts to higher q values, which obviously reflects a decreasing mean distance between neighboring particles. The lower interaction peaks for $ChEO_{10}$ can be related to the higher polydispersity of the system than that for $ChEO_{15}$. The interaction radius, r_i, at infinite dilution extracted from $S(q)$ is 6.7 nm for $ChEO_{15}$ and 8.8 nm for $ChEO_{10}$, being compatible with $D_{max}/2$ obtained from PDDF. This consistency ensures the validity of the separation of $P(q)$ and $S(q)$ by the GIFT calculation. This also supports the formation of elongated micelles with a length distribution in the water/$ChEO_{10}$ systems.

Temperature-Induced Structural Change. We measured the temperature dependence of the density and the sound velocity in solution for 5, 10, 15, and 20 wt % water/$ChEO_n$ binary systems ($n = 10$ and 15) in the temperature range $5 \leq T/°C \leq 70$. It is usually more convenient to use the relative difference of the solution density, ρ, to that of the solvent water, ρ_w, and also that of sound velocity in the solution, v, to that in the solvent water, v_w. We therefore calculated the two derivatives

$$D_\rho = \frac{d(\rho - \rho_W)}{dT} = \frac{d\Delta\rho}{dT} \tag{20}$$

and

$$D_S = \frac{d[(v - v_W)/v_W]}{dT} = \frac{dS}{dT} \tag{21}$$

where $S=(v\text{-}v_w)/v_w$ is the so-called sound number. In Figure 9a−d, D_ρ/ϕ_S and D_S/ϕ_S, the derivatives of the relative density and the sound number normalized by the volume fraction of the surfactants for 5, 10, 15, and 20 wt % water/$ChEO_n$ binary systems ($n = 10$ and 15) are presented. We can expect that the structural change of the solutions is reflected in the change of D_ρ/ϕ_S and D_S/ϕ_S.[21] As for the water/$ChEO_{15}$ systems, both D_ρ/ϕ_S and D_S/ϕ_S shown in Figure 9, panels a and b, show smooth temperature dependence with no singular point in $5 \leq T/°C \leq 70$ for all of the investigated concentrations. In contrast, these quantities for the water/$ChEO_{10}$ system exhibit characteristic behavior, indicating occurrence of temperature-induced structural changes in the W_m phase. D_ρ/ϕ_S of the 5 wt % water/$ChEO_{10}$ system shows a small peak at∼45 °C as indicated by an arrow in Figure 9c, the temperature at which a peak appears shifts to lower values with increasing W_S. In parallel, D_S/ϕ_S shown in Figure 9d also shows a small bump at the corresponding temperatures. As shown in Figure 10a, the zero shear viscosity of a 2.5 wt % $ChEO_{10}$ solution starts a steep increase at ∼45 °C. The rising viscosity with increasing temperature is usually attributed to the formation of elongated micelles, i.e., one-dimensional micellar growth.[3,33] We found that the behavior of D_ρ/ϕ_S at higher temperature is strongly correlated with a phase boundary determined with visual observation. For a 20% water/$ChEO_{10}$ system, when a phase separation occurs, inhomogeneity of the sample at the macroscopic level leads to a sudden divergence of D_ρ/ϕ_S, resulting in a strong oscillation of D_ρ/ϕ_S. With a further increase of the temperature, D_ρ/ϕ_S for 5, 10, and 15 wt % water/$ChEO_{10}$ solutions shows the second peak at the temperature where a high viscosity solution is formed, and subsequently exhibits a divergence because density measurements with a DMA5000 cannot be correct for high viscosities.[21] In the water/$ChEO_{15}$ systems, a highly viscous solution is not formed even at very high temperatures and the W_m phase region spread over the wide temperature range of $T > 100$ °C. It appears that a growth of a rod-micelle is not promoted in the water/$ChEO_{15}$ systems, and as a result, homogeneity of the systems is higher than that in water/$ChEO_{10}$ systems.

In the water/$ChEO_{10}$ system, at low concentrations, the micellar solutions have a viscosity comparable to that of water. However, with increasing temperature, the viscosity of the micellar solution begins to increase, and a viscoelastic system is formed at high temperature even at a low surfactant concentration, as shown in the Figure 10b. The viscoelastic solution shows shear-birefringence. Variation of zero-shear viscosity of a 2.5 wt % $ChEO_{10}$ solution as a function of temperature obtained from rheological measurement is shown in Figure 10a. The increase of the viscosity is attributed to a decrease of the interfacial cross-sectional area (a_s) of the surfactant headgroup with increasing temperature. Such a decrease of a_S would induce a packing constrain in the lipophilic core of the aggregate, thereby inducing a unidimensional micellar growth leading to the formation of long and flexible cylindrical aggregates, often called "wormlike" micelles. The oscillatory shear rheological behavior of the system at 65 °C (Figure 10b), which can be described by the Maxwell model of the viscoelastic fluid, is a typical rheological pattern of the wormlike micelles entangled to form a transient network.

Hydration of Oxyethylene Chain. We determined the complex dielectric spectra of 5, 10, and 15 wt % water/$ChEO_n$ binary systems ($n = 10$ and 15) at 25 °C in the frequency range $0.1 \leq \nu/GHz \leq 20$ by the use of Time Domain Reflectometry (TDR).[17−19] For the better resolution, the data were obtained with the TDMD method introduced by Sato et al.[19] The typical spectrum is displayed in Figure 11. Upon addition of surfactant to water, a small contribution emerges around ∼3GHz. As the results of the fitting procedure, we found that a superposition of a Cole−Cole (j=1) and a Debye (j=2) relaxation

$$\epsilon^*(\nu) = \epsilon_\infty + \frac{\Delta\epsilon_1}{1 + (i2\pi\nu\tau_1)^\beta} + \frac{\Delta\epsilon_2}{1 + i2\pi\nu\tau_2} \tag{22}$$

gives the best description to the spectra.

$\Delta\epsilon_1$ exhibits a linear-like increase against surfactant molar concentration, c, which proves that the $j = 1$ process is related

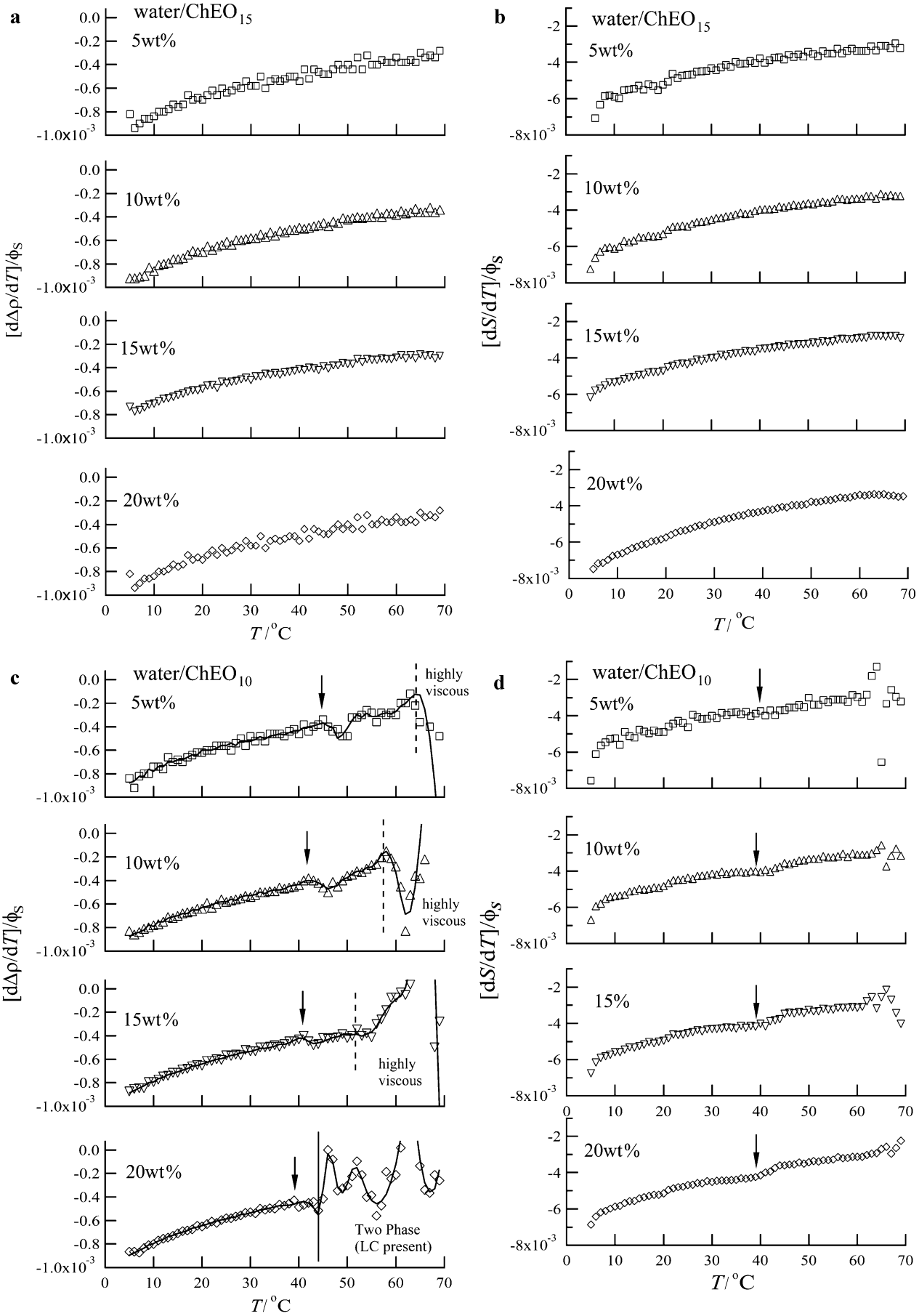

Figure 9. Temperature differential of the relative density and the sound number for 5, 10, 15, and 20 wt % water/ChEO$_n$ binary systems ($n = 10$ and 15) normalized by the surfactant volume fraction obtained in the temperature range $5 \leq T/°C \leq 70$.

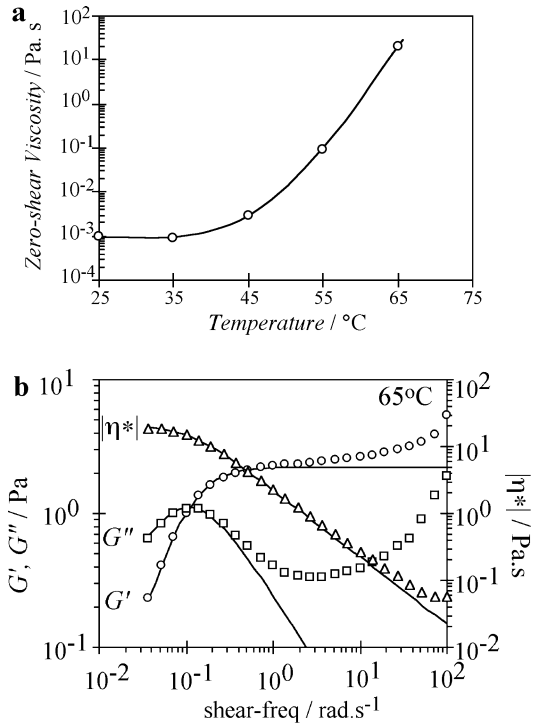

Figure 10. (a) Zero shear viscosity (η_0) of a 0.03M $ChEO_{10}$ solution as a function of temperature, and (b) variation of elastic modulus (G'), viscous modulus (G'') and modulus of complex viscosity (η^*) as a function of oscillatory-shear frequency for a 0.03M $ChEO_{10}$ solution at 65 °C. The solid lines represent the Maxwell fit.

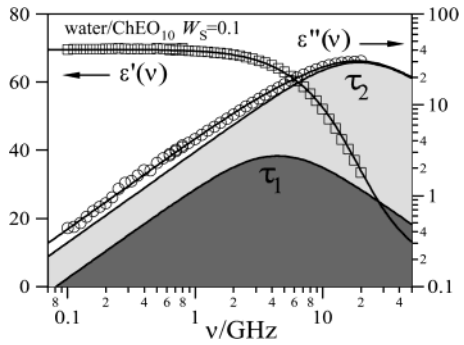

Figure 11. Dielectric dispersion, $\epsilon'(\nu)$, and loss, $\epsilon''(\nu)$, spectrum of a 10 wt % $ChEO_{10}$ aqueous solution at 25 °C in the frequency range $0.1 \leq \nu/\mathrm{GHz} \leq 20$ measured by the use of time domain reflectometry (TDR) with the time-window divided modified direct (TDMD) method.[19]

to kinetics of micelles. However, if we interpret this low-frequency process as the rotational diffusion of the micelles referring to the Storks-Einstein-Debye equation, the observed τ_1 is apparently too small for a spherical-like particle with a radius of ~7 nm, but we found that τ_1 is quite compatible with the relaxation time of aqueous solutions of oligo(ethylene glycol)s at the similar ratio of water and oxyethylene unit.[17] We can therefore assign the low-frequency process to kinetics of hydrophilic layer of micelles including the motion of hydrated oxyethylene chain and hydrated water. The relaxation time of the high-frequency process, τ_2, is identical with that of pure water, $\tau_w = 8.3$ps, and almost independent of the concentration, and the amplitude, $\Delta\epsilon_2$, is smoothly decreased from that for pure water with decreasing water content. The process can be clearly attributed to the cooperative rearrangement of H-bond network of bulk water.

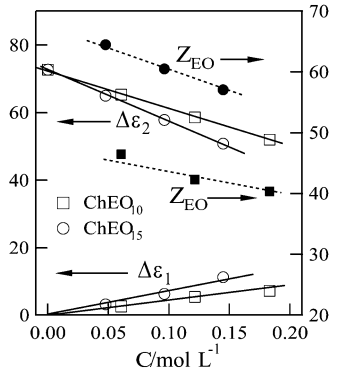

Figure 12. Concentration dependence of the relaxation amplitudes, $\Delta\epsilon_j$ ($j = 1$ and 2) for 5, 10, and 15 wt % water/$ChEO_n$ binary systems ($n = 10$ and 15) at 25 °C, and the effective hydration number of oxyethylene chain, Z_{EO}, for $ChEO_{10}$ and $ChEO_{15}$ plotted against molar concentration of the surfactant, C.

We estimated the hydration number of oxyethylene chain in the W_m phase using the Cavell equation[19]

$$\Delta\epsilon_i = \frac{\epsilon}{3(\epsilon + (1-\epsilon)A_i)} \frac{N_A}{k_B T \epsilon_0} \frac{g_i \mu_{Gi}^2}{(1-\alpha_i f_i)^2} c_i \qquad (23)$$

which relates the relaxation amplitude of the ith process, $\Delta\epsilon_i$, to the concentration of the relaxation species, c_i, where μ_{Gi} is a gas-phase dipole moment, α_i a polarizability, f_i the field factor, A_i the shape parameter of the reaction field, ϵ the static permittivity, g_i the dipole−dipole correlation factor, k_B the Boltzmann constant, N_A the Avogadro's number, and ϵ_0 the vacuum permittivity.

From eq 23, the solvent-process-normalized Cavell equation, which yields the apparent solvent concentration for the solution at the solute concentration c, $c_w^{app}(c)$, can be obtained as

$$c_W^{app}(c) = c_W(c)\frac{g_W(c)}{g_W(0)} = \frac{\epsilon(0)(2\epsilon(c)+1)}{\epsilon(c)(2\epsilon(0)+1)} \frac{(1-\alpha_W f_W(c))^2}{(1-\alpha_W f_W(0))^2} \frac{\Delta\epsilon_W(c)}{\Delta\epsilon_W(0)} c_W(0) \qquad (24)$$

where $\Delta\epsilon_W(0) = 72.8$ and $\Delta\epsilon_W(c) = \Delta\epsilon_2(c)$. Assuming a spherical water molecule ($A_i = 1/3$) with a radius $r = 0.1425$ nm and a polarizability of water molecule $\alpha_W = 1.607 \times 10^{-40}$ $C\,m^2/V$, the apparent concentration of bulk water, $c_W(c)^{app}$, was deduced. We can define the effective hydration number of oxyethylene chain, Z_{EO},[34] by converting the difference between the analytical water concentration, $c_W(c)$, and the apparent concentration, $c_W^{app}(c)$, to the number of water molecules per solute surfactant

$$Z_{EO} = (c_W(c) - c_W^{app}(c))/c \qquad (25)$$

Z_{EO} corresponds to the number water molecules that cannot contribute to the bulk water process due to hydration to surfactant molecules. In Figure 12, the relaxation amplitude for the micellar process, $\Delta\epsilon_1$, and that for bulk water process, $\Delta\epsilon_2$ and Z_{EO} are plotted against molar concentration of the surfactant. We obtained $Z_{EO} = 40-45$ for $ChEO_{10}$ and 55−65 for $ChEO_{15}$. This means that approximately 4−4.5 water molecules are hydrated per oxyethylene unit. The values are quite consistent with those obtained in NMR studies.[35,36] Based of the analysis of Z_{EO}, bulk water does not exist any more in $W_S > \sim 0.5$.

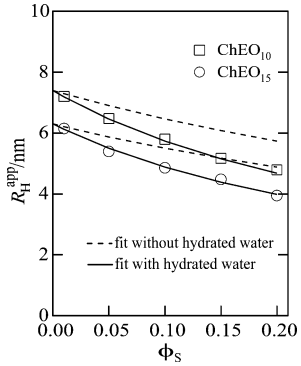

Figure 13. Apparent hydrodynamic radius, R_H^{app}, for the water/$ChEO_{15}$ and the water/$ChEO_{10}$ systems obtained by dynamic light scattering (DLS) at 25 °C, plotted against the surfactant volume fraction, ϕ_S.

Figure 13 shows the concentration dependence of the apparent hydrodynamic radius of micelles in 1, 5, 10, 15, and 20 wt % water/$ChEO_n$ ($n = 10$ and 15) solutions, R_H^{app}, obtained by DLS. With the rise of W_S, R_H^{app} decreases, which appears to be due to the effects of inter-micellar interactions. The concentration dependence of R_H^{app} can normally be described as

$$R_H^{app} = \frac{R_H}{1 + A\phi_S} \tag{26}$$

where R_H is the hydrodynamic radius at infinite dilution, ϕ_S is the volume fraction of the particle, and A is a coefficient. $R_H = 7.4$ nm for $ChEO_{10}$ and $R_H = 6.3$ nm for $ChEO_{15}$ were obtained. The fact that R_H for $ChEO_{10}$ exceeds that of $ChEO_{15}$ well supports the results of SAXS, the formation of short rod-micelles in the water/$ChEO_{10}$ system. For a hard sphere, $A = 1.56$ is expected for eq 26.[37] However, in actual, we found $A \sim 2.9$ for both $ChEO_{10}$ and $ChEO_{15}$, approximately twice larger than expected. Lindner et al. reported quite similar phenomenon for a triblock copolymer P94 in water.[16] If, as revealed by DRS measurements, ~45 hydrated water molecules for each $ChEO_{10}$ molecule and ~60 hydrated water molecules for each $ChEO_{15}$ molecule are included to the volume fraction of the particle, ϕ_S, i.e., if hydrated water molecules are regarded as the constituent of micelles and thus $\phi_S \sim W_S$ in eq 26 is replaced by

$$\phi_S' \sim \phi_S[(M_S + 18n_W)/M_S] \tag{27}$$

where n_W is the number of hydrated molecule per surfactant molecule and M_S is the molecular weight of the surfactant, eq 26 with $\phi_S' \sim 2\phi_S$ and $A = 1.56$ can well explain the concentration dependence of R_H^{app}. If the effective volume fraction, ϕ_{eff}, obtained from the calculation of $S(q)$ by the GIFT method is twice larger than the actual volume fraction of surfactant for $ChEO_{15}$, and a bit less than twice but larger by the factor of ~1.5 for $ChEO_{10}$. This supports the results of DLS and DRS. We can conclude that hydrated water molecules should be considered as the components of diffusive particles. Based of the analysis of the hydration number, fully hydrated micelles are present with nearly no bulk water molecules at W_S~0.5, which corresponds to the boundary of the I_1 phase and the H_1 phase. A further reduction of the water content, as a result, a reduction of hydrated water and incomplete hydration of the oxyethylene chains, lead to a reduction of the headgroup repulsion.

IV. Conclusion

We have thoroughly investigated the phase behavior and the micellar structures in the water/poly(oxyethylene) cholesteryl ether binary systems. We found that the water/$ChEO_n$ ($n = 10$ and 15) systems exhibit a number of novel phase behavior due to the effects of a bulky and nonflexible hydrophobic part of the surfactants and intricate hydrophobic−hydrophilic balance controlled by the different EO chain length. Both systems show extremely wide intermediate phase region on the lower surfactant concentration side of the L_α region, in which the rectangular ribbon (R_1) phase with the centered rectangular symmetry, *cmm* or *cm*, has been identified.

In the water/$ChEO_{15}$ system, with increasing water content, the packing parameter and axial ratio of an aggregate in the R_1 region are smoothly decreased and finally converges respectively to 1/2 and 1, the characteristics of the H_1 phase. The findings clearly demonstrate that R_1 phase acts as a "distorted" hexagonal phase. The phase behavior of the water/$ChEO_{10}$ system, however, is far more complicated. For example, H_1 and I_1 phases are missing. In addition, in the R_1 region, when W_S is reduced, a sudden elongation of ribbonlike aggregates occurs at $W_S \sim 0.7$, which is opposite to a general rule of increasing interfacial curvature with increasing water content. After showing the maximum packing parameter ~0.67, just corresponding to the threshold of discontinuous and bicontinuous structures, at $W_S \sim 0.5$ the R_1 phase is changed into a different type of liquid crystalline phase, where the SAXS reflections cannot be well indexed to any known space group for liquid crystalline phases.

The GIFT analysis of the SAXS data for the W_m solution obtained in the absolute scale, reinforced by rheology, DLS, and densimetry, revealed that spherical micelles are formed in the water/$ChEO_{15}$ system, whose structure is nearly independent of temperature and concentration, but $ChEO_{10}$ forms a short-rod micelle in water at ambient temperature and rodlike micelles are rapidly grown with the rise of temperature, leading to the formation of a viscoelastic micellar phase. The results of DLS and DRS indicate that about four hydrated water molecules per oxyethylene unit should be counted in a constituent of the micelles.

Acknowledgment. T.S. gratefully acknowledges helpful discussions on the packing parameter with Prof. B. W. Ninham and on the hydration number analysis with Dr. R. Buchner. This work was partly supported by the 21st century center of excellence (COE) program, Waseda University, "Physics of self-organization systems composed of multicomponents" from Japan Society for the Promotion of Science (JSPS).

References and Notes

(1) Kim, W.-J.; Yang, S.-M. *J. Colloid Interface Sci.* **2000**, *232*, 225.
(2) Khatory, A.; Lequeux, F.; Kern, F.; Candau, S. J. *Langmuir* **1993**, *9*, 1456.
(3) Acharya, D. P.; Kunieda, H. *J. Phys. Chem. B* **2003**, *107*, 10168.
(4) Shigeta, K.; Olsson, U.; Kunieda, H.; *Langmuir* **2001**, *17*, 4717.
(5) Kunieda, H.; Uddin, Md. H.; Horii, M.; Furukawa, H.; Harashima, A. *J. Phys. Chem. B* **2001**, *105*, 5419.
(6) Kunieda, H.; Kabir, H.; Aramaki, K.; Shigeta, K. *J. Mol. Liq.* **2001**, *90*, 157.
(7) Glatter, O.; Fritz, G.; Lindner, H.; Brunner-Popela, J.; Mittelbach, R.; Strey, R.; Egelhaaf, S. U. *Langmuir* **2000**, *16*, 8692.
(8) Glatter, O. *J. Appl. Crystallogr.* **1980**, *13*, 577.
(9) Glatter, O.; Strey, R.; Schubert, K.-V.; Kaler, E. W. *Ber. Bunsen-Ges. Phys. Chem.* **1996**, *100*, 323.
(10) Strey, R.; Glatter, O.; Schubert, K.-V.; Kaler, E. W. *J. Chem. Phys.* **1996**, *105*, 1175.
(11) Iampietro, D. J.; Brasher, L.L.; Kaler., E.W.; Stradner, A.; Glatter, O. *J. Phys. Chem. B* **1998**, *102*, 3105.
(12) Brunner-Popela, J.; Glatter, O. *J. Appl. Crystallogr.* **1997**, *30*, 431.

(13) Weyerich, B.; Brunner-Popela, J.; Glatter, O.*J. Appl. Crystallogr.* **1999**, *32*, 197.
(14) Bergmann, A.; Orthaber, D.; Scherf, G.; Glatter, O. *J. Appl. Crystallogr.* **2000**, 33, 869.
(15) Orthaber, D.; Bergmann, A.; Glatter, O. *J. Appl. Crystallogr.* **2000**, *33*, 218.
(16) Lindner, H.; Scherf, G.; Glatter, O. *Phys. Rev. E* **2003**, *67*, 061402−1.
(17) Sato, T.; Niwa, H.; Chiba, A.; Nozaki, R. *J. Chem. Phys.* **1998**, *108*, 4138.
(18) Sato, T.; Buchner, R. *J. Chem. Phys.* **2003**, *119*, 10789.
(19) Sato, T.; Buchner, R. *J. Phys. Chem. A* in press.
(20) Buchner, R.; Hefter, G. T.; May, P. M. *J. Phys. Chem. A* **1999**, *103*, 1.
(21) Fritz, G.; Scherf, G.; Glatter, O. *J. Phys. Chem. B* **2000**, *104*, 3463.
(22) Holmes, M. C. *Curr. Opin. Colloid Interface Sci.* **1998**, *3*, 485.
(23) Funari, S. S.; Holmes, M. C.; Tiddy, G. J. T. *J. Phys. Chem.* **1992**, *96*, 11029.
(24) Funari, S. S.; Holmes, M. C.; Tiddy, G. J. T. *J. Phys. Chem.* **1994**, *98*, 3015.
(25) Fairhurst, C. E.; Holmes, M. C.; Leaver, M. S. *Langmuir* **1997**, *13*, 4964.
(26) Burgoyne, J.; Holmes, M. C.; Tiddy, G. J. T. *J. Phys. Chem.* **1995**, *99*, 6054.
(27) Israelachvili, J.; Mitchell, D. J.; Ninham. B. W. *J. Chem. Soc., Faraday Trans. 2* **1976**, *72*, 1525.
(28) Mitchell, D. J.; Ninham. B. W. *J. Chem. Soc., Faraday Trans. 2* **1981**, *77*, 601.
(29) Hyde, S.; Andersson, S.; Larsson, K.; Blum, Z.; Landh, T.; Lidin, S.; Ninham, B. W. *The Language of Shape*; Elsevier: Amsterdam, 1997; Chapter 4.
(30) Gustafsson, S.; Quist, P.-O. *J. Colloid interface Sci.* **1996**, *180*, 564.
(31) Hagslätt, H.; Söderman, O.; Jönsson, B. *Liq. Cryst.* **1992**, *12*, 667.
(32) Hagslätt, H.; Fontell, K. *J. Colloid Interface Sci.* **1994**, *165*, 431.
(33) Lehner, D.; Lindner, H.; Glatter, O. *Langmuir* **2000**, *16*, 1689.
(34) (a) Buchner, R. Private communication. (b)Schrödle, S.; Buchner, R.; Kunz, W. Unpublished result.
(35) Nilsson, P. G.; Lindman, B. *J. Phys. Chem.* **1983**, *87*, 4756.
(36) Klose, G.; Eienblätter, St; Galle, J.; Islamov, A.; Dietrich, U. *Langmuir* **1995**, *11*, 2889.
(37) Fijnaut, H. M. *J. Chem. Phys.* **1981**, *74*, 6857.